Hindawi
Journal of Nanomaterials
Volume 2019, Article ID 4269348, 11 pages
https://doi.org/10.1155/2019/4269348

Research Article

Computational Modeling of Biosynthesized Gold Nanoparticles in Black *Camellia sinensis* Leaf Extract

Parvaneh Shabanzadeh,[1,2] **Rubiyah Yusof**,[1,2] **Kamyar Shameli**,[2] **Abdollah Hajalilou**,[3] **and Shidrokh Goudarzi**[2]

[1]*Center for Artificial Intelligence and Robotics, Universiti Teknologi Malaysia, 54100 Kuala Lumpur, Malaysia*
[2]*Malaysia-Japan International Institute of Technology (MJIIT), Universiti Teknologi Malaysia, Jalan Sultan Yahya Petra (Jalan Semarak), 54100 Kuala Lumpur, Malaysia*
[3]*Faculty of Mechanical Engineering, Department of Materials Engineering, Tabriz University, Iran*

Correspondence should be addressed to Parvaneh Shabanzadeh; parvaneh.shabanzade@gmail.com and Rubiyah Yusof; rubiyah.kl@utm.my

Received 29 May 2018; Revised 9 October 2018; Accepted 17 October 2018; Published 14 January 2019

Academic Editor: Ovidiu Ersen

In this research, gold nanoparticles (Au-NPs) are biosynthesized from tetrachloroaurate ($AuCl_4^-$) aqueous solution through a simple and ecofriendly route using water extract of black *Camellia sinensis* leaf (*C. sinensis* L.) which acted as a reductant and stabilizer simultaneously. The prepared gold nanoparticles are characterized using UV-visible spectroscopy, X-ray diffraction (XRD), and transmission electron microscopy (TEM). Also, determination of the accurate predictor model for chemical reactions is particularly important because of high cost of the chemical materials and measurement devices. While the artificial neural networks (ANNs) are one of the appropriate tools to forecast any phenomena, due to the low number of data set related to chemical experimental was caused to provide appropriate model is a time-consuming iterative process. With the aim to improve the accuracy of the ANN model and overcome the local convergence of this problem, a global search technique, biogeography-based optimization (BBO) method which integrated by chaotic map is employed. The improved model showed minimum mean squared error (MSE) of 0.0134 and maximum coefficient of determination (R^2) equal to 0.9822 compared with several other famous ANN training algorithm, utilizing output experimental data obtained from biosynthesis proceeding.

1. Introduction

Nanotechnology is an expanding and emerging field of research that has been developing interest which focuses on the advancement of biosynthetic and synthetic techniques for preparation of nanoparticles over the globe with giant force in forming nanosolstice because of their wide applications. Due to the totally new or improved properties of nanoparticles, their applications are becoming quickly on different fronts like biomedical, pharmaceutical, catalysis, medicate conveyance, and antimicrobial [1].

Gold, platinum, silver, titanium, palladium, aluminum, iron, and copper including the different nanoparticles gained enormous consideration late because of their imperative significance [2]. Among the aforesaid metal nanoparticles, gold nanoparticle (Au-NP) is the most important due to its long history of medicinal use like treatment of cancer and arthritis [3] and due to their biocompatibility.

The biosynthesis of nanoparticles, which shows a relation between nanotechnology and biotechnology, has received enhance attention due to growing need to develop eco-friendly technologies for nanomaterial green synthesis. The gold nanoparticle biosynthesis has been reported using plant tissues, such as leaf, root, stem bark, and flower and also bacteria, fungi, and actinomycetes. Among other methods for biosynthesis of gold nanoparticles, extracellular synthesis has received much attention as it eliminates various steps [4]. The chemical, physical, and even the use of microbes have less attention than biosynthetic method using plant extracts for synthesis of nanomaterials. Due to absence of

any detrimental for the environment and the cost of production, biosynthesis method is more suitable for nanoscale metals [5].

Tea has been used socially and habitually and a medical drink of people since 3000 B.C. The scientific name of tea is *Camellia sinensis*, the species of a plant that is used as green and black leaves for the production of tea [6]. Tea leaves contain many compounds such as polyphenols of the flavonoid type (e.g., theaflavins, catechins), polysaccharides, vitamins, volatile oils, minerals, and purines and xanthine alkaloids type such as theobromine, caffeine, and theophylline [7]. Theaflavins in black tea and/or catechin in green tea are known as a stronger antioxidant compound [8].

The precise prediction model of chemical reaction based on experimental data is a significant subject because this concern could save the cost of numerous experiments. Artificial neural networks (ANNs) are one of the powerful predictor tools that have been widely used in the various science and medical and engineering and control in an effectively manner [9–12]. ANN is composed from several elements known as neurons and is an idea of data processing inspired from human neural network [13]. The main feature of ANN is the capability of finding the correlation between the input and output data without any previous knowledge and ability of dealing with manifold variables as well as linear and nonlinear relationships [14]. In recent years, with the aim to overcome the drawbacks of backpropagation-based training of ANNs, such as slow convergence rate, large computational time, and getting stuck at local minima, some of evolutionary optimization algorithms, such as the genetic algorithm [11], the particle swarm optimization method [15, 16], and artificial bee colony [17], have been applied for training ANN and others [18, 19]. Also, the chaos theory [20] has been used to many aspects of the optimization science [21–25]. The chaotic maps can improve optimization algorithms by the ability of escaping to fall in local solutions and increasing the speed of convergence to reach global solution [26].

The objective of this paper is to reach an intelligent ANN model involving a combination of improved biogeography-based optimization (BBO) method [27] by chaos-based, with acceptable performance and simple topology, for forecasting the size of Au-NPs which obtained in biosynthesis process. The effect of reaction variables, volume of *C. sinensis* L. extract, reaction temperature, stirring time, and volume of $AuCl_4^-$ was investigated on the size of Au-NPs. Also, the interrelations between each variable and the objective parameter were presented.

2. Materials and Methods

2.1. Materials. The black tea leaves (*C. sinensis* L.) was collected from the plantation in Cameron Highlands, Malaysia. Analytical grade tetrachloroaurate salt ($HAuCl_4$, 99.98%) was purchased from Sigma-Aldrich, USA, and was used as a gold precursor. All solutions were kept in the dark place to eschew any photochemical reactions and also were freshly prepared using double distilled water (DD water).

2.2. Extract Preparation. After drying, the black *C. sinensis* L. was milled into a powder form, stored in a black container, and kept at 25°C until further analyses. The finely ground *C. sinensis* L. (3.0 g) was heated in 100 mL of deionized water at 60°C for 20 min. Using a vacuum pump and Whatman filter paper no. 1 sample was isolated and residue reextracted again. The volatile solvent was removed using a rotary vacuum evaporator at 45°C. The concentrated aqueous extracts were kept in dark container at 5°C until used.

2.3. Synthesis of Au-NPs in C. sinensis L. Extract. In this procedure, 0.6 g of *C. sinensis* L. crude extract was added to 100 mL double distilled water with normal stirring for 1 h. Then, certain volume of *C. sinensis* L. (1, 2, 5, 10, and 20 mL) mixed with different volumes of $AuCl_4^-$ (1×10^{-3} M) (1, 2, 5, 10, 20, and 30 mL) and mixed at different temperature (27, 35, 40, 50, 60, and 70°C) for variable stirring time (0.5, 1.5, 3, 6, and 9 h). The Au-NPs were gradually begun to produce during these periods. The Au-NPs in *C. sinensis* L. emulsion obtained were kept at 4°C. The obtained Au-NP suspensions were centrifuged at 30,000 rpm for 15 minutes and washed to remove gold ion residue. The precipitated Au-NPs were then dried at 35°C under vacuum condition.

2.4. Characterization Methods and Instruments. The Au-NPs/*C. sinensis* L. were characterized using physical and chemical instruments such as X-ray diffraction (XRD), transmission electron microscopy (TEM), and UV-vis spectroscopy. The structures of the Au-NPs were studied using the XRD (Philips, X'Pert, Cu Kα). TEM images were obtained with a Hitachi H-7100® electron microscope (Hitachi High-Technologies Corporation, Tokyo, Japan). Mean particle size distributions of Au-NPs were determined using the UTHSCSA Image Tool® Version 3.00 program. The UV-vis spectra were recorded over the range of 300–800 nm with an H.UV 1650 PC-SHIMADZU B.

2.5. Artificial Neural Network Methodology. The methods of artificial intelligence have greatly been utilized in the different fields of the chemical application [28–30]. In neural network, each input is multiplied by the synaptic weight, added together, and applied with an activation function and then ANNs are trained repeatedly till the best relationship between the input and output values is obtained and reached a model after a sufficient number of learning repetitions or training known as epochs [31].

After the training step, the ANN presentation has generalization capacity with new input values to predict, simulate, and find the condition identified as testing procedure. The performance and accuracy of neural network is evaluated by two factors utilized to focus on configuration errors, coefficient of determination (R^2), and mean square error (MSE):

$$\begin{aligned} \mathrm{MSE} &= \frac{1}{n\sum_{i=1}^{n}\left(\mathrm{po}_i - \mathrm{do}_i\right)^2}, \\ R^2 &= 1 - \frac{\sum_{i=1}^{n}\left(\mathrm{po}_i - \mathrm{do}_i\right)^2}{\sum_{i=1}^{n}\left(\mathrm{po}_i - \mathrm{do}_m\right)^2}, \end{aligned} \tag{1}$$

where do_i and po_i are desired output and predicted output results from ANN, respectively. The a_m is the average amount of output over the entire number sample n. The coefficient of determination (R^2) can be considered as performance criterion of the network by the linear regression of predicted values of ANN from the exact measured data. The accuracy of network based on test partition is index threshold of trained network. Therefore, the closer value to zero was the criteria to decide which model was better.

The following equation shows that the ranges of input variables are various, when each of the variables was normalized in the range of −1 to 1.

$$XN_i = \frac{(X_i - \text{Min } X)}{(\text{Max } X - \text{Min } X)} * 2 - 1 \quad i = 1, \ldots, \dim (X), \quad (2)$$

where XN_i denotes ith normalized input of (X), X_i is ith input variable of X, and Min X and Max X show minimum and maximum input variable of X, respectively.

2.6. Biogeography-Based Optimization (BBO) Method. Biogeography-based optimization method was suggested by Simon [27], which is a population and stochastic optimization technique for solving multimodal optimization. The BBO method is inspired from the concept of biogeography, which deals with the distribution of species that depend on different factors, such as rainfall, diversity of vegetation, diversity of topographic features, land area, and temperature [32]. A larger number of species are found in suitable areas compared with that of a less suitable area. The regions that are well suited as residents for species are evaluated by a habitat suitability index (HSI) (cost function), and the variables that characterize habitability are called suitability index variable (SIV) (variables). The large numbers of species on high HSI islands have many opportunities to emigrate into neighboring habitats with less number of species and share their good characteristics with those habitats, thus archiving a high species immigration rate. In BBO method, a poor solution is introduced to an island with low HSI and conversely a good solution is introduced to an island with high HSI. The poor solutions accept many new features from good solutions and improve their quality. Then, the shared features of the good solution still remain in the high HSI solutions. BBO consists of two main steps: migration and mutation. Migration step is a probabilistic operator that is intended to improve a candidate solution [33, 34]. The migration step is consisting of two different types: emigration and immigration, and that for each solution in each iteration, the rates of these types are adaptively indicated based on the fitness of the solution. In BBO, each candidate solution ha_i has its own emigration rate μ_i, and immigration rate λi is as follows:

$$\mu_i = A\left(\frac{\gamma(i)}{ns}\right), \quad (3)$$

$$\lambda_i = B\left(1 - \frac{\gamma(i)}{ns}\right), \quad (4)$$

where ns is the population size and $\gamma(i)$ presents the rank of i th individual in a ranked list which has been sorted based on the fitness of the population from the worst fitness to the best one (1 is worst and ns is best). Also, A and B are the maximum possible emigration and immigration rates, which are typically set to one. For sharing information between candidate solutions (habitats), different methods have been recommended in [35, 36], where migration is proposed by

$$ha_i(\text{SIV}) = \delta * ha_i(\text{SIV}) + (1 - \delta) * ha_j(\text{SIV}), \quad (5)$$

where δ could be a random, deterministic number, or proportional to the relative fitness of the solutions ha_i and ha_j but it should be between 0 and 1. This means that in equation (5) (feature solution), SIV of ha_i comes from a combination of its own SIV and the emigrating solution is SIV.

Also, the mutation step is important; its purpose is to increase diversity among the population. The mutation rate is calculated in [27]:

$$M_i = M_{\max}\left(\frac{1 - \partial_i}{\partial_{\max}}\right), \quad (6)$$

$$ha_i(\text{SIV}) = ha_i(\text{SIV}) + 0.02 * (\text{VarMax} - \text{VarMin}), \quad (7)$$

where ∂_i is the solution probability, $\partial_{\max} = \max_i \partial_i$, $i = 1, \ldots, ns$, and that ns is the population size and $M_{\max}$ is a user-defined parameter.

Based on the above description, the main steps of the BBO algorithm can be described as follows:

Step 1. Initialization. Set initial parameters: the number of iterations (necessary for the termination criterion) and population size, which indicates the number of habitats and create a random set of habitats (population), number of design variables, maximum immigration and emigration rates, and mutation coefficient

Step 2. Evaluation. Compute corresponding HSI values and rank them on the basis of fitness

Step 3. Update Parameters. Update the immigration rate λ_i and emigration rate μ_i for each island/solution. Bad solutions have low emigration rates and high immigration rates, whereas good solutions have high emigration rates and low immigration rates

Step 4. Select Islands. Probabilistically select the immigration islands based on the immigration rates and select the emigrating islands based on the emigration rates via roulette wheel selection

Step 5. Migration Phase. Migrate randomly selected features (SIVs) based on the selected islands in the previous step, based on equations (3–5)

Step 6. Mutation Phase. Probabilistically carry out mutation based on the mutation probability for each solution, i.e., based on equations (6 and 7)

Step 7. Termination Criteria. Check if the termination criterion step is met and then stop; otherwise, go to Step 2

2.7. Chaotic Local Search. Initially, chaos theory was introduced by Hénon [20] and Lorenz [37]. Chaos is a common nonlinear occurrence in nature, where it is completely reflects the complexity of the system. Chaos maps can be applied in optimization methods to avoid entrapment in local optimal [25, 38]. Logistic map was introduced by May [39] that appears in nonlinear dynamics of biological population evidencing chaotic behavior. Also, this map demonstrates how complex behavior arises from simple deterministic system without the need of any random sequence and whose equation is as follows:

$$x_{n+1} = \delta x_n (1 - x_n), \tag{8}$$

where x_n is nth chaotic number and where n presents the iteration number. If $x_0 \epsilon (0, 1)$, then $x_n \exists (0, 1)$ so that $x_0 \notin \{0.0, 0.25, 0.5, 0.75, 1.0\}$. $\delta = 4$ was considered in this research. It has presented in [25] that the logistic map perfectly has improved quality of solution, which obtained from global optimization method. Therefore, the logistic map was used in this research as local search algorithm to improve optimization solution $x^{\text{op}} = (x_1^{\text{op}}, x_2^{\text{op}}, \ldots, x_T^{\text{op}})$ which has been obtained from BBO method. Then, the chaotic local search algorithm is as follows:

Step 1. Set variance range $[\propto_t, \beta_t], t = 1, \ldots, T$ for each optimal variable $x_t^{\text{op}}, t = 1, \ldots T$ so that $x_t^{\text{op}} - \varepsilon < \propto_t$ and $x_t^{\text{op}} + \varepsilon > \beta_t$, where ε is specified radius of chaos search. Also, set $k = 1$, where k is the iteration index and specify the maximum number of iteration $K\gamma_1$.

Step 2. Generate chaotic variable γ_t by using equation (8).

Step 3. Map chaotic variable γ_t into variance range of each optimal variable is shown as follows:

$$x_t^k = x_t^{\text{op}} - \varepsilon + 2\varepsilon\gamma_k \quad \forall t = 1, \ldots T. \tag{9}$$

Step 4. Update the best solution. If $f(x^k) < f(x^{\text{op}})$, then $x^{\text{op}} = x^k$.

Step 5. Termination criteria. If the termination criterion is met, then stop and output x^{op} is the best solution as the final result. Otherwise $k = k + 1$ and go to Step 3.

3. Results and Discussion

3.1. UV-vis Spectroscopy Analysis. Reduction of gold salt to Au-NPs during exposure to aqueous extract of *C. sinensis* L. could be followed by the change of color (Figures 1(a) and 1(b)). The fresh suspension of *C. sinensis* L. was light brownish in color (Figure 1(a)). After adding the gold ions into the aqueous extract of *C. sinensis* L., emulsion color turned to ruby red with the change in condition of reaction (Figure 1(b)). UV-vis spectroscopy has proven to be a useful spectroscopic method for the detection of synthesized metallic nanoparticles; for this reason, biosynthesized Au-NPs were studied by this method. The formation of Au-NPs was followed by measuring the surface plasmon resonance of the *C. sinensis* L. and Au-NPs/*C. sinensis* L. emulsions over the wavelength range from 250 to 800 nm. Figure 1 shows that Au-NPs started forming when $AuCl_4^-$ reacted directly with *C. sinensis* L. at a room temperature. The surface plasmon resonance band for Au-NPs absorbed at around 515–572 nm which indicates the spherical structure for these nanoparticles [40].

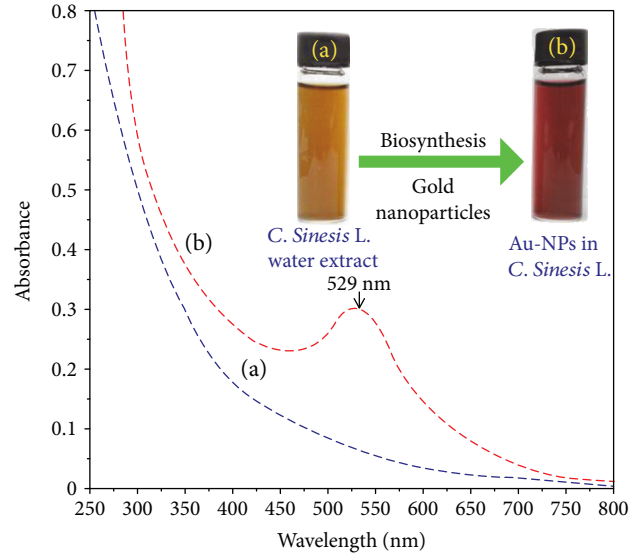

Figure 1: UV-vis absorption spectra and photographs of (a) *C. sinensis* L. water extract and (b) Au-NPs in *C. sinensis* L. suspension.

3.2. X-ray Diffraction. X-ray diffraction (XRD) pattern showed that the synthesized Au-NPs are formed in *C. sinensis* L. extract (Figure 2). A broad diffraction peak was observed at 22.77°, which is attributed to *C. sinensis* L. The XRD patterns of Au-NPs indicated that the structure of Au-NPs is a face-centered cubic. The peaks of XRD at 2θ of 38.28°, 44.58°, 64.82°, 77.66°, and 81.87° could be attributed to the 111, 200, 220, 311, and 222 crystallographic planes of gold crystals, respectively [41, 42]. Based on XRD reference code no. 01-089-3697, the main crystalline phase was gold and there were no obvious any extra peaks in the XRD patterns.

3.3. Morphology Study. TEM image and particle distributions of Au-NPs on *C. sinensis* L. extract are shown in Figure 3. The TEM image and their size distribution have shown that mean diameter and standard deviation of Au-NPs were around 23.33 ± 6.69 nm. In the high magnification of TEM, it can be observed clearly that Au-NPs are surrounded by the *C. sinensis* L. extract. Based on the obtained results, the shape and size of the Au-NPs can also be controlled by *C.*

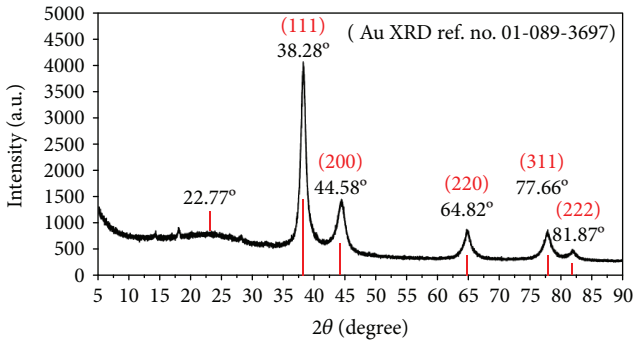

FIGURE 2: XRD patterns of Au-NPs synthesized in *C. sinensis* L. aqueous extract.

sinensis L. aqueous extract. This result approved that the size of the synthesized Au-NPs depended to the stirring reaction time, reaction temperature, volume of *C. sinensis* L. extract, and volume of $AuCl_4^-$.

3.4. Computational Models. In continuation, all computational programs are written in the MATLAB software, to make a representation for predicting the size of Au-NPs. A multilayer feedforward ANN with backpropagation (BP) algorithm was applied for modeling of experimental results so that the values of *C. sinensis* L. extract, reaction temperature, stirring time, and volume of $AuCl_4^-$ as input variables and size of Au-NPs as output variable were used. Figure 4 shows the graphical proposed ANN model.

Therefore, the data set was split and shuffled into 80%, 20% shares for training and testing of the ANN model. A neural network with one hidden layer could reach suitable performance, while more increasing the number of hidden layers causes overfitting and more computational complexity [42, 43]. MSE, R^2 as indexes of network performance were used to evaluate the best fitting representation [44]. The optimum network structure was chosen with a minimum value of MSE and maximum coefficient of determination R^2. Therefore, MLP neural network with 4-3-1 architecture and hyperbolic tangent sigmoid transfer function [45] was chosen as neural network model. The hyperbolic tangent sigmoid function is as follows:

$$f(x) = 2/\left(1 + e^{-2x}\right) - 1, \quad -1 \le f(x) \le 1. \tag{10}$$

With the aim of obtaining the optimal neural network representation, the method for training should be decided, which means that finding the best training method to adjust weights and biases should be determined. Then in Figure 5(a), a general configuration of the developed ANN model is explained.

Therefore, five prominent training BP methods, Levenberg-Marquardt (LM) BP [46], gradient descent BP, BFGS quasi-Newton BP [47], BFGS quasi-Newton Fletcher-Reeves conjugate gradient (FCG) algorithm [48], and Bayesian regulation BP (BR) [49] and BBO method and improved BBO (IBBO) algorithm by chaos local search method, were used with the intention of achieving the lowest possible MSE and greater coefficient of determination R^2. Table 1 shows mean and standard deviation of MSE and R^2 for 50 runs of each training algorithm. Then, the ANN models which trained with BBO and especially IBBO reached the best results with the lowest MSE and higher coefficient of determination compared with the other methods which were used in this research.

In the lowest amount for MSE related to training data, test and all data were reached by the ANN model that was trained by IBBO method with the following values: 0.00755, 0.01343, and 0.00873. Figure 6 shows the accuracy of the best ANN model, and R^2, for the test and train, and all data set have values of 0.98229, 0.98117, and 0.98028, respectively, which trained with IBBO method which error trend promises no overfitting happened and that has an acceptable performance and great agreement between predicted and actual values. Therefore, it is notable that from the outstanding performance of learning, the proposed model has an acceptable error (MSE of 0.06842) and high accuracy (R^2 of 0.82075) in the case of prediction data set that signifies the generalization of the proposed model.

Equation (11) represents the fitness function for the ANN model that correlates the input variables with output:

$$\begin{aligned}
&\mathrm{ANN} = \mathrm{tansig}(\mathrm{WH}(\mathrm{tansig}(\mathrm{WI}[x_1; x_2; x_3; x_4] + \mathrm{BH}) + \mathrm{BO})),\\
&\mathrm{WI} = \begin{Bmatrix} -5.3192 & 2.7021 & -1.3427 & -0.22362 \\ -2.3258 & 1.4597 & 0.60989 & 0.4856 \\ 9.0262 & -0.55644 & 6.646 & 3.9701 \end{Bmatrix},\\
&\mathrm{WH} = \{0.751980.570880.62378\},\\
&\mathrm{BH} = \begin{Bmatrix} -1.0479 \\ -3.5605 \\ -0.22429 \end{Bmatrix},\\
&\mathrm{BO} = 0.24604,
\end{aligned} \tag{11}$$

where x_1, x_2, x_3, and x_4 show the input variables (WI, WH), which are matrices of weights for input and hidden layers and (BO, BH) are the matrixes of biases for output and hidden layers, respectively, that can be useful for the prediction of the size of Au-NPs in other situations without a need to do any real experiment by other researchers.

The relation between input and output variables was investigated separately which results confirm that condition for other input variables was constant. The results of Figure 7 present that the measurement of the size of Au-NPs decreases rapidly with the increasing the amount of volume of *C. sinensis* L. extract. Inversely increasing the values of the stirring time, temperature of reaction, and volume of $AuCl_4^-$ will increase the size of Au-NPs.

Also, the effects of each two combinations of input variables and on the size of nanoparticles were investigated and presented in Figures 8(a)–8(f). The effects of stirring time and temperature of reaction on output are displayed in Figure 8(a). The points of light and dark blue, yellow, and red area show more effectiveness of increasing property of

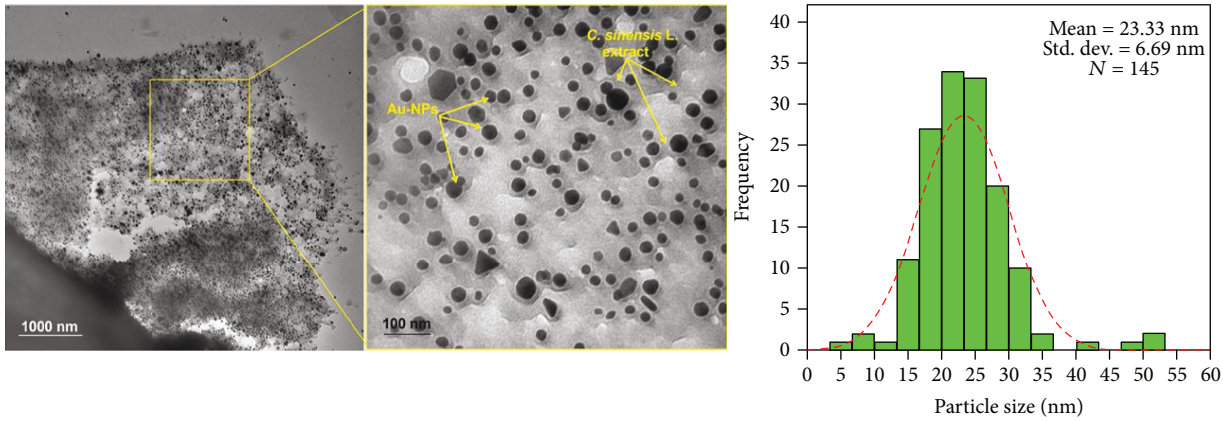

Figure 3: TEM image and corresponding size distribution of Au-NPs in *C. sinensis* L. extract.

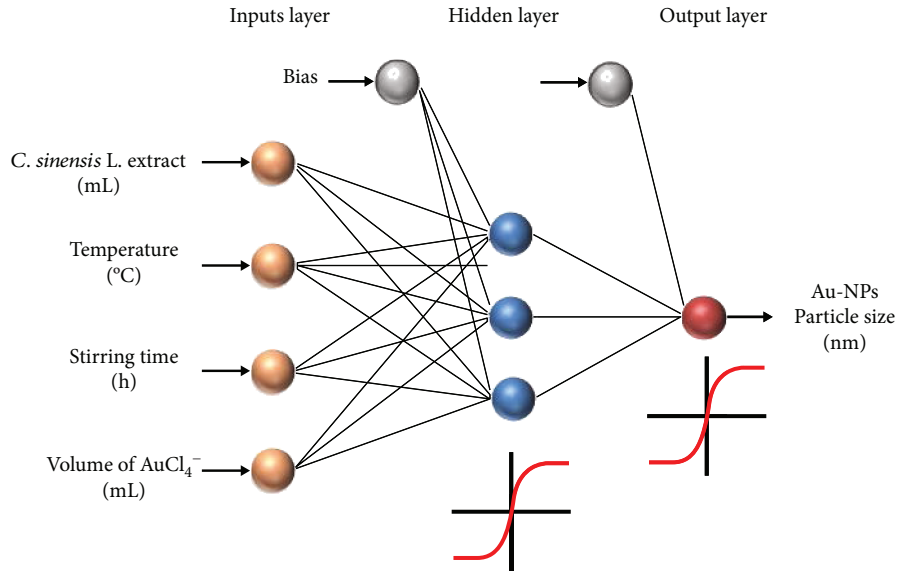

Figure 4: The graphical proposed ANN model.

value of reaction temperature compared with the stirring time. Therefore, the minimum size of Au-NPs happened during less than 1 hour of stirring time at 27°C and also maximum size of Au-NPs has arisen in 9 hours at 70°C. The impacts of estimations of the volume of *C. sinensis* L. extract and reaction temperature are displayed in Figure 8(b). The points were indicated in red, yellow, and light and dark blue areas; it can be concluded that "increasing the volume of *C. sinensis* L. extract has a direct effect on the reduction property and more effectiveness than the value of reaction temperature which has the increasing size of Au-NPs."

The minimum size of Au-NPs is accrued in the experimental condition at 27°C and 20 mL of *C. sinensis* L. extract. Also, the Au-NPs' maximum size was outcropped at 70°C and 1 mL of *C. sinensis* L. extract.

A change in the volume of $AuCl_4^-$ and the reaction temperature and its effect on the size of the Au-NPs is shown in Figure 8(c). The points in red area show the increasing property of both variables on the size of Au-NPs. The minimum size of Au-NPs was synthesized in less than 5 mL of $AuCl_4^-$ at 27°C, and also the maximum size of Au-NP was prepared at 70°C and 30 mL of $AuCl_4^-$.

The effects of the volume of $AuCl_4^-$ and stirring time of reaction on the size of nanoparticles are shown in Figure 8(d). The points of light and dark blue, yellow, and red areas show more increasing property of stirring time than the volume of $AuCl_4^-$. Then, maximum size of Au-NPs is synthesized after 9 hours of stirring time and 30 mL of $AuCl_4^-$ and minimum size of Au-NPs is prepared after 0.5 hour of stirring time and less than 5 mL of $AuCl_4^-$.

The size of Au-NPs based on the values of *C. sinensis* L. extract volume and stirring time is presented in Figure 8(e). The results showed that the volume of *C. sinensis* L. extract is more effective compared to the reaction stirring time in the control size of Au-NPs.

In Figure 8(f), the size of Au-NPs based on the volume of *C. sinensis* L. extract and volume of $AuCl_4^-$ is represented. The figure shows "the volume of *C. sinensis* L. extract has

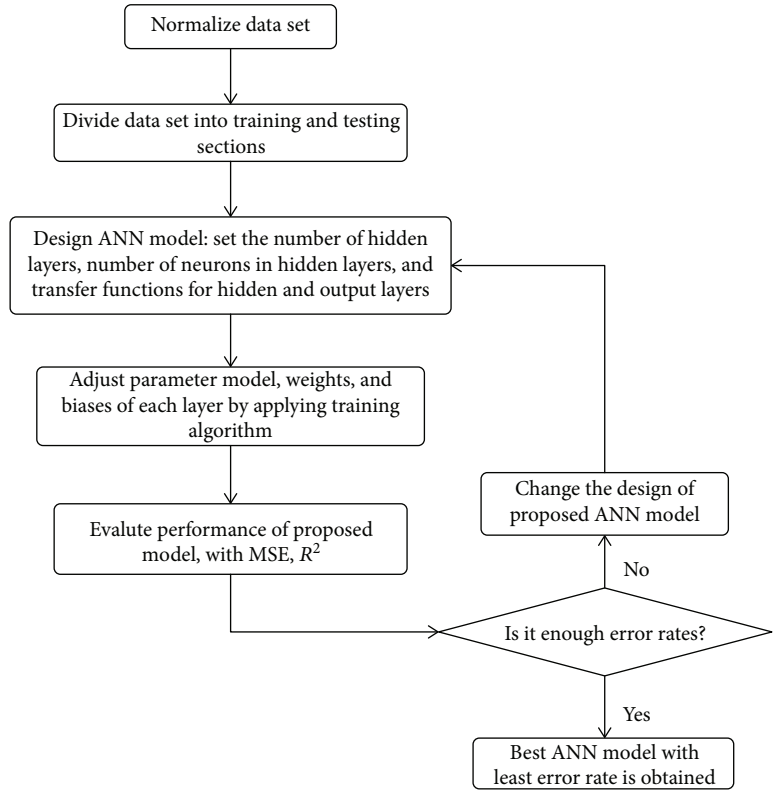

Figure 5: The general configuration of the proposed ANN model.

Table 1: Comparison of proposed method with other ANN training algorithm methods (the results have been run over 50 times).

Training algorithm		Error of MSE for train data set	Error of MSE test data set	Error of MSE for all data set	R^2 train data set	R^2 test data set	R^2 all data set
BBO	Mean	0.02788	0.13976	0.050253	0.94158	0.8502	0.90211
	Std.	0.00994	0.084918	0.02284	0.030358	0.095858	0.05488
IBBO	Mean	0.0168	0.06842	0.027123	0.9655	0.82075	0.9426
	Std.	0.00870	0.04921	0.013165	0.01536	0.16422	0.02109
LM	Mean	0.82218	0.73313	0.80437	0.20929	0.071544	0.19152
	Std.	0.45563	0.50258	0.43994	0.55242	0.59973	0.53191
BR	Mean	0.89932	0.91367	0.90219	0.08041	0.16773	0.08368
	Std.	0.54795	0.61153	0.53461	0.6546	0.55121	0.62575
BFGS	Mean	0.84558	0.66035	0.80853	0.00926	−0.10722	−0.01068
	Std.	0.45243	0.45886	0.45193	0.59425	0.66829	0.60458
GDA	Mean	0.6908	0.75501	0.70364	0.08736	−0.03519	0.06249
	Std.	0.44392	0.5596	0.45799	0.62295	0.64031	0.619
FCG	Mean	0.68511	0.83815	0.71572	0.15577	0.22267	0.19553
	Std.	0.48889	0.73824	0.53275	0.56779	0.59573	0.5627

decreasing property and more effectiveness than volume of $AuCl_4^-$ which has the increasing property on size of Au-NPs." Then, the points of Figure 8(f) show that the maximum size of Au-NPs has occurred 30 mL of $AuCl_4^-$ and 1 mL of *C. sinensis* L. extract, while the minimum size of Au-NPs has occurred 20 mL of *C. sinensis* L and less than 5 mL of $AuCl_4^-$.

4. Conclusion

In this research, an optimized ANN model was proposed in order to estimate accurate size of Au-NPs synthesized by green method. A number of various input parameters such as the volume of *C. sinensis* L. extract, temperature of reaction, stirring time, and volume of $AuCl_4^-$ were introduced

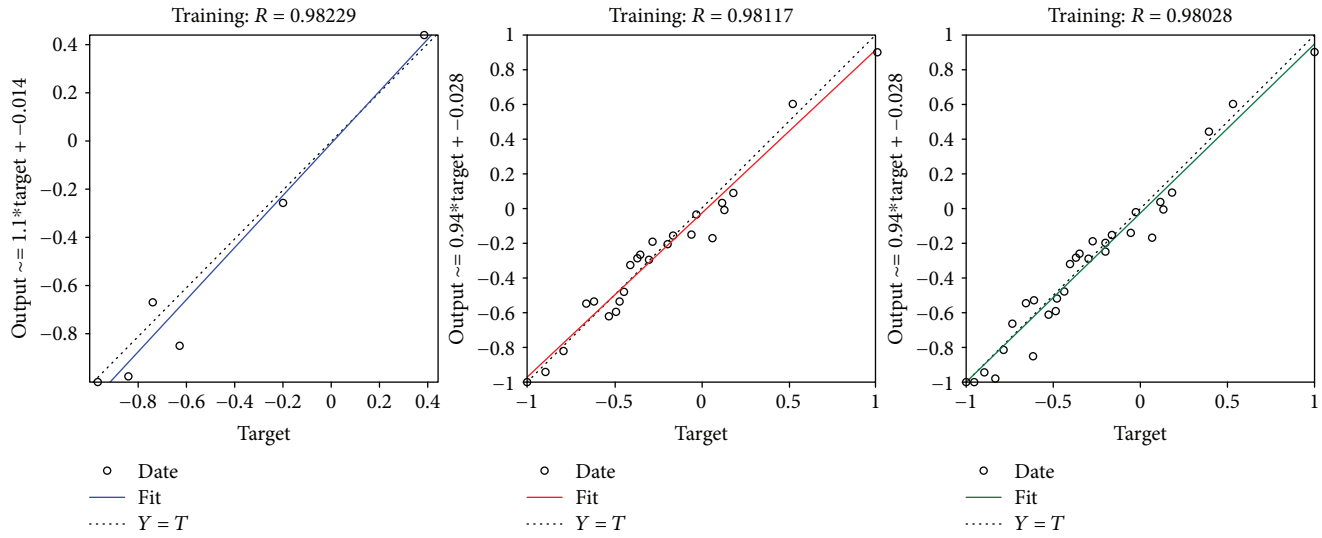

Figure 6: The scatter plots of the ANN model predicted versus actual values for training, testing, and all data sets.

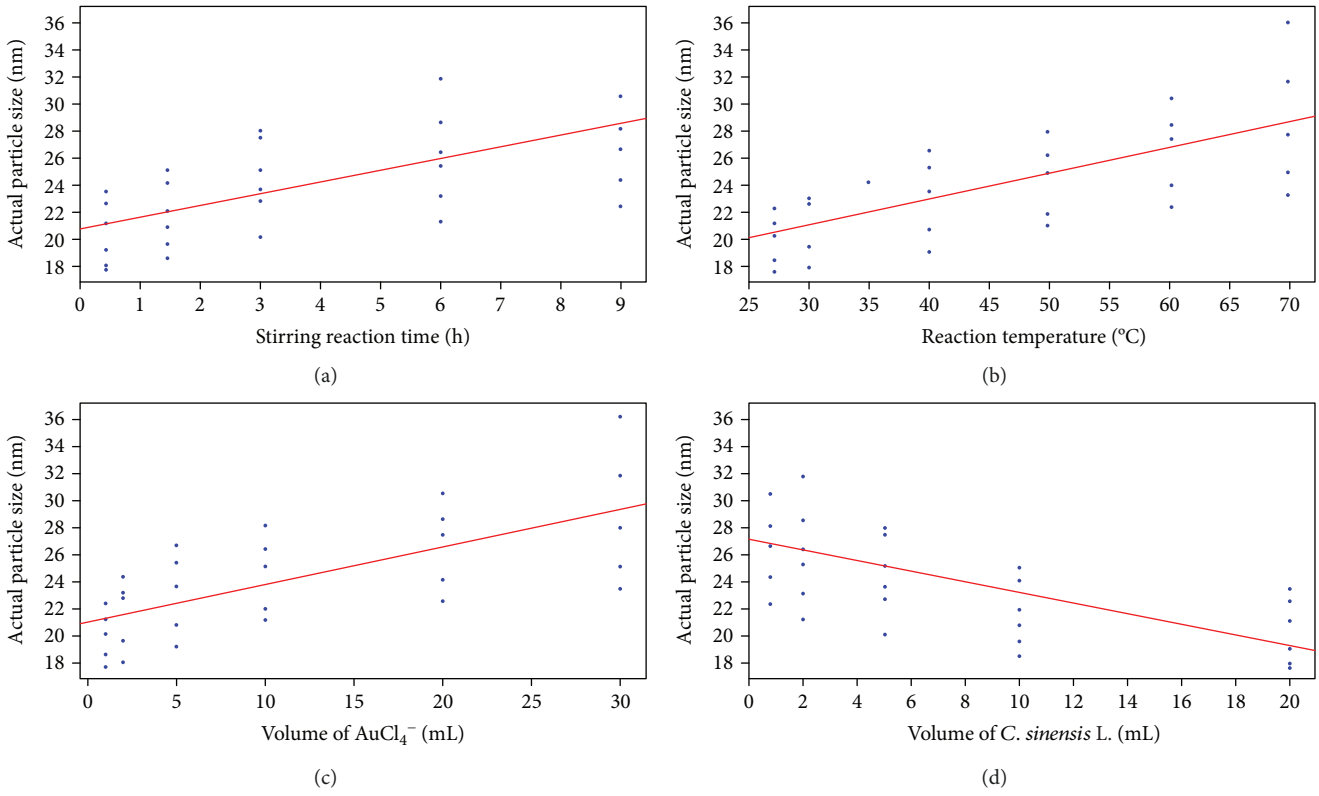

Figure 7: Two-dimensional plots on effects of the volume of *C. sinensis* L. extract (a), temperature reaction (b), string time (c), and volume of $AuCl_4^-$ (d) on the size of Au-NPs.

that measure the size of Au-NPs by using the ANN model and compare with actual results that obtained from TEM. Subsequently, a combination of chaos and BBO methods was applied to weight training of the ANN model. It was also disclosed that IBBO training algorithm with 4-3-1 architecture and using the sigmoid transfer function for hidden and output layers yields the better results than other well-known training algorithms. So, IBBO algorithm can be a useful candidate for training ANNs. Also, the close fitting of simulated values to experimental data as satisfactory confirmed the performance of the trained ANN model. It was divulged that increasing the reaction of temperature, volume of $AuCl_4^-$, and stirring reaction time leads to increased size of nanoparticles. The results indicated this fact that with

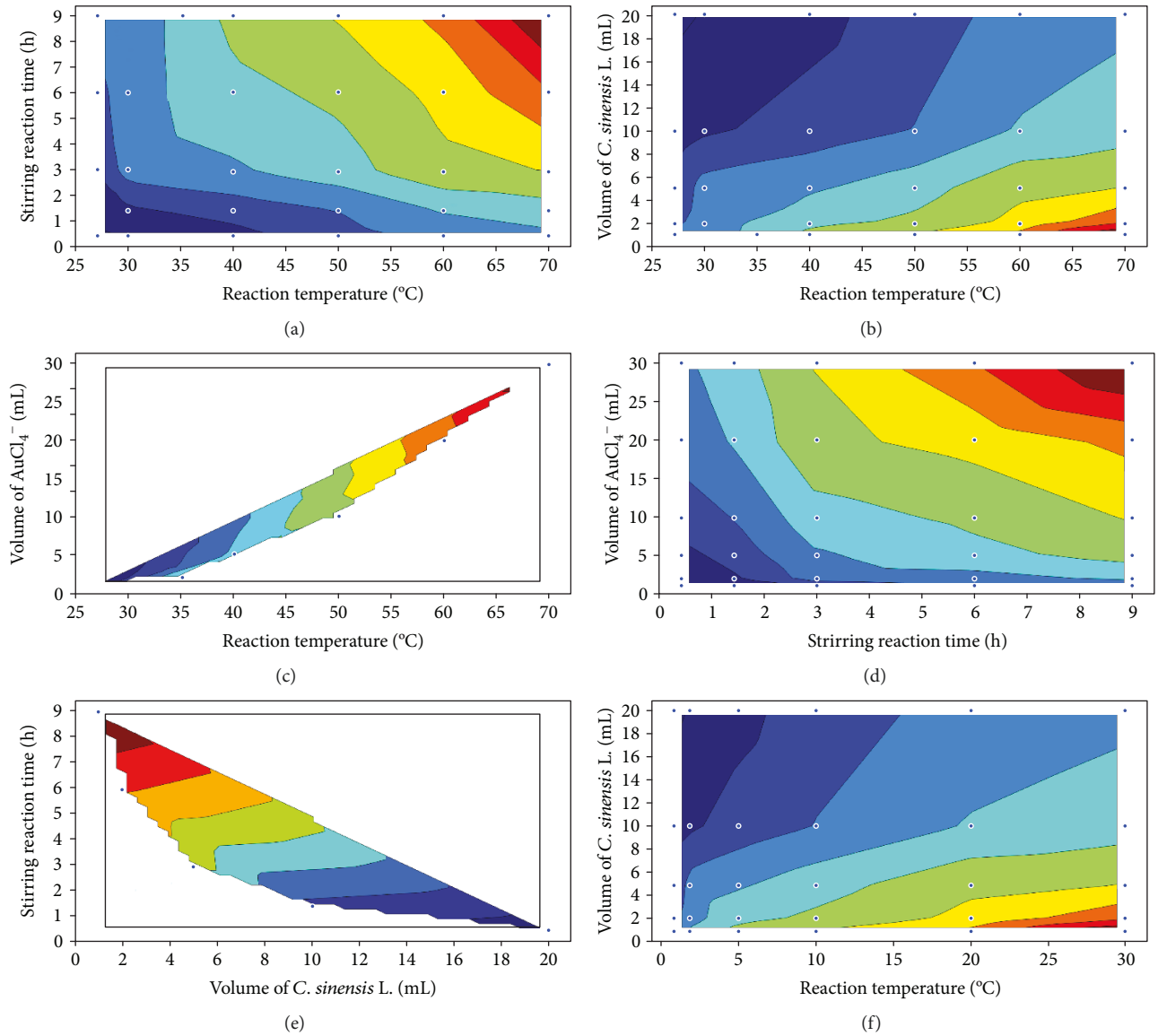

Figure 8: Two-dimensional surfaces show the effects of values of the reaction temperature and stirring time (a), effects of values of the volume of *C. sinensis* L. extract and reaction temperature (b), effects of values of the volume of $AuCl_4^-$ and temperature of reaction (c), effects of values of the volume of $AuCl_4^-$ and stirring time (d), effects of values of the stirring time and volume of *C. sinensis* L. extract (e), and effects of values of the volumes of *C. sinensis* L. extract and $AuCl_4^-$ (f), on the size of Au-NPs.

the increasing volume of *C. sinensis* L. extract, the size of Au-NPs decreases. The minimum and maximum sizes of Au-NPs are shown in experimental condition as follows: 25 to 70°C, 0.5 to 9 hours for stirring time, 20 to 2 mL of *C. sinensis* L. extract, and 5 to 30 mL of $AuCl_4^-$, respectively (around 7 to 36 nm). As a result, the proposed model can be used as a valuable and alternative tool for the prediction of the size of the synthesized Au-NPs.

Data Availability

The data used to support the findings of this study are available from the corresponding author upon request.

Conflicts of Interest

The authors declare that there is no conflict of interest regarding the publication of this paper.

Acknowledgments

The authors would like to thank the Ministry of Education Malaysia for funding this research project through a Research University Grant of Universiti Teknologi Malaysia (UTM), project titled "Multi Modal Vehicle Security System (MMVSS)" (4L659). Also, we thank to the Research Management Center (RMC) of UTM for providing an excellent research environment in which to complete this work.

References

[1] S. Ahmed, M. Ahmad, B. L. Swami, and S. Ikram, "A review on plants extract mediated synthesis of silver nanoparticles for antimicrobial applications: a green expertise," *Journal of Advanced Research*, vol. 7, no. 1, pp. 17–28, 2016.

[2] S. Chaturvedi, P. N. Dave, and N. K. Shah, "Applications of nano-catalyst in new era," *Journal of Saudi Chemical Society*, vol. 16, no. 3, pp. 307–325, 2012.

[3] R. R. Arvizo, S. Bhattacharyya, R. A. Kudgus, K. Giri, R. Bhattacharya, and P. Mukherjee, "Intrinsic therapeutic applications of noble metal nanoparticles: past, present and future," *Chemical Society Reviews*, vol. 41, no. 7, pp. 2943–2970, 2012.

[4] K. Shameli, M. B. Ahmad, A. Zamanian et al., "Green biosynthesis of silver nanoparticles using Curcuma longa tuber powder," *International Journal of Nanomedicine*, vol. 7, pp. 5603–5610, 2012.

[5] K. Shameli, M. B. Ahmad, P. Shabanzadeh et al., "Effect of Curcuma longa tuber powder extract on size of silver nanoparticles prepared by green method," *Research on Chemical Intermediates*, vol. 40, no. 3, pp. 1313–1325, 2014.

[6] A. B. Sharangi, "Medicinal and therapeutic potentialities of tea (Camellia sinensis L.)–a review," *Food Research International*, vol. 42, no. 5-6, pp. 529–535, 2009.

[7] S. Konwar Boruah, P. Kumar Boruah, P. Sarma, C. Medhi, and O. Kumar Medhi, "Green synthesis of gold nanoparticles using Camellia sinensis and kinetics of the reaction," *Advanced Materials Letters*, vol. 3, no. 6, pp. 481–486, 2012.

[8] E. W. C. Chan, E. Y. Soh, P. P. Tie, and Y. P. Law, "Antioxidant and antibacterial properties of green, black, and herbal teas of Camellia sinensis," *Pharmacognosy Research*, vol. 3, no. 4, pp. 266–272, 2011.

[9] J. Cheng, X. Wang, T. Si et al., "Maximum burning rate and fixed carbon burnout efficiency of power coal blends predicted with back-propagation neural network models," *Fuel*, vol. 172, pp. 170–177, 2016.

[10] Ö. Çelik, A. Teke, and H. B. Yıldırım, "The optimized artificial neural network model with Levenberg-Marquardt algorithm for global solar radiation estimation in Eastern Mediterranean Region of Turkey," *Journal of Cleaner Production*, vol. 116, pp. 1–12, 2016.

[11] M. B. Takahashi, J. C. Rocha, and E. G. F. Núñez, "Optimization of artificial neural network by genetic algorithm for describing viral production from uniform design data," *Process Biochemistry*, vol. 51, no. 3, pp. 422–430, 2016.

[12] N. Zavrtanik, J. Prosen, M. Tušar, and G. Turk, "The use of artificial neural networks for modeling air void content in aggregate mixture," *Automation in Construction*, vol. 63, pp. 155–161, 2016.

[13] S. S. Haykin, *Neural Networks: A Comprehensive Foundation*, Prentice-Hall, Upper Saddle River, NJ, USA, 1999.

[14] V. Chandwani, V. Agrawal, and R. Nagar, "Modeling slump of ready mix concrete using genetic algorithms assisted training of artificial neural networks," *Expert Systems with Applications*, vol. 42, no. 2, pp. 885–893, 2015.

[15] E. Momeni, D. J. Armaghani, M. Hajihassani, and M. F. M. Amin, "Prediction of uniaxial compressive strength of rock samples using hybrid particle swarm optimization-based artificial neural networks," *Measurement*, vol. 60, pp. 50–63, 2015.

[16] P. Shabanzadeh, R. Yusof, and K. Shameli, "Modeling of biosynthesized silver nanoparticles in Vitex negundo L. extract by artificial neural network," *RSC Advances*, vol. 5, no. 106, pp. 87277–87285, 2015.

[17] S. M. Awan, M. Aslam, Z. A. Khan, and H. Saeed, "An efficient model based on artificial bee colony optimization algorithm with neural networks for electric load forecasting," *Neural Computing and Applications*, vol. 25, no. 7-8, pp. 1967–1978, 2014.

[18] J. Kumaran and G. Ravi, "Long-term forecasting of electrical energy using ANN and HSA," *International Review on Modelling and Simulations (IREMOS)*, vol. 7, no. 3, p. 489, 2014.

[19] J. Kumaran and G. Ravi, "Teaching learning based optimization of ANN for electrical energy forecasting," *Australian Journal of Basic and Applied Sciences*, vol. 8, no. 16, pp. 56–63, 2014.

[20] M. Hénon, "A two-dimensional mapping with a strange attractor," *Communications in Mathematical Physics*, vol. 50, no. 1, pp. 69–77, 1976.

[21] G.-G. Wang, A. Hossein Gandomi, and A. Hossein Alavi, "A chaotic particle-swarm krill herd algorithm for global numerical optimization," *Kybernetes*, vol. 42, no. 6, pp. 962–978, 2013.

[22] L. Wang, D. Z. Zheng, and Q. S. Lin, "Survey on chaotic optimization methods," *Computing Technology and Automation*, vol. 20, no. 1, pp. 1–5, 2001.

[23] A. H. Gandomi, X.-S. Yang, S. Talatahari, and A. H. Alavi, "Firefly algorithm with chaos," *Communications in Nonlinear Science and Numerical Simulation*, vol. 18, no. 1, pp. 89–98, 2013.

[24] M. A. El-Shorbagy, A. A. Mousa, and S. M. Nasr, "A chaos-based evolutionary algorithm for general nonlinear programming problems," *Chaos, Solitons & Fractals*, vol. 85, pp. 8–21, 2016.

[25] S. Saremi, S. R. Mirjalili, and A. Lewis, "Biogeography-based optimisation with chaos," *Neural Computing and Applications*, vol. 25, no. 5, pp. 1077–1097, 2014.

[26] P. Ammaruekarat and P. Meesad, "A chaos search for multiobjective memetic algorithm," in *2011 International conference on information and electronics engineering*, pp. 140–144, Harbin, China, 2011.

[27] D. Simon, "Biogeography-based optimization," *IEEE Transactions on Evolutionary Computation*, vol. 12, no. 6, pp. 702–713, 2008.

[28] M. Sadrzadeh, T. Mohammadi, J. Ivakpour, and N. Kasiri, "Separation of lead ions from wastewater using electrodialysis: comparing mathematical and neural network modeling," *Chemical Engineering Journal*, vol. 144, no. 3, pp. 431–441, 2008.

[29] S. W. Tsang and C. Y. Jim, "Applying artificial intelligence modeling to optimize green roof irrigation," *Energy and Buildings*, vol. 127, pp. 360–369, 2016.

[30] P. Shabanzadeh, R. Yusof, and K. Shameli, "Artificial neural network for modeling the size of silver nanoparticles' prepared in montmorillonite/starch bionanocomposites," *Journal of Industrial and Engineering Chemistry*, vol. 24, pp. 42–50, 2015.

[31] S. Jaiswal, E. R. Benson, J. C. Bernard, and G. L. Van Wicklen, "Neural network modelling and sensitivity analysis of a mechanical poultry catching system," *Biosystems Engineering*, vol. 92, no. 1, pp. 59–68, 2005.

[32] J. Kumaran and G. Ravi, "Long-term sector-wise electrical energy forecasting using artificial neural network and biogeography-based optimization," *Electric Power Components and Systems*, vol. 43, no. 11, pp. 1225–1235, 2015.

[33] S. Yang, R. X. Wu, M. Wang, and L. Jiao, "Evolutionary clustering based vector quantization and SPIHT coding for image compression," *Pattern Recognition Letters*, vol. 31, no. 13, pp. 1773–1780, 2010.

[34] M. Ergezer, D. Simon, and D. Du, "Oppositional biogeography-based optimization," in *2009 IEEE International Conference on Systems, Man and Cybernetics*, pp. 1009–1014, San Antonio, Texas, USA, October 2009.

[35] S. Yazdani, J. Shanbehzadeh, and E. Aminian, "Feature subset selection using constrained binary/integer biogeography-based optimization," *ISA Transactions*, vol. 52, no. 3, pp. 383–390, 2013.

[36] M. Yazdani and F. Jolai, "Lion optimization algorithm (LOA): a nature-inspired metaheuristic algorithm," *Journal of Computational Design and Engineering*, vol. 3, no. 1, pp. 24–36, 2016.

[37] E. N. Lorenz, *The Essence of Chaos*, University of Washington Press, 1996.

[38] L. dos Santos Coelho and V. C. Mariani, "A novel chaotic particle swarm optimization approach using Hénon map and implicit filtering local search for economic load dispatch," *Chaos, Solitons & Fractals*, vol. 39, no. 2, pp. 510–518, 2009.

[39] R. M. May, "Simple mathematical models with very complicated dynamics," *Nature*, vol. 261, no. 5560, pp. 459–467, 1976.

[40] V. Amendola and M. Meneghetti, "Size evaluation of gold nanoparticles by UV−vis spectroscopy," *Journal of Physical Chemistry C*, vol. 113, no. 11, pp. 4277–4285, 2009.

[41] K. Shameli, M. B. Ahmad, E. A. J. Al-Mulla, P. Shabanzadeh, and S. Bagheri, "Antibacterial effect of silver nanoparticles on talc composites," *Research on Chemical Intermediates*, vol. 41, no. 1, pp. 251–263, 2015.

[42] N. I. S. B. Abdullah, M. B. Ahmad, and K. Shameli, "Biosynthesis of silver nanoparticles using Artocarpus elasticus stem bark extract," *Chemistry Central Journal*, vol. 9, no. 1, p. 61, 2015.

[43] M. Rezakazemi, S. Razavi, T. Mohammadi, and A. G. Nazari, "Simulation and determination of optimum conditions of pervaporative dehydration of isopropanol process using synthesized PVA–APTEOS/TEOS nanocomposite membranes by means of expert systems," *Journal of Membrane Science*, vol. 379, no. 1-2, pp. 224–232, 2011.

[44] Y. Yasin, F. B. H. Ahmad, M. Ghaffari-Moghaddam, and M. Khajeh, "Application of a hybrid artificial neural network–genetic algorithm approach to optimize the lead ions removal from aqueous solutions using intercalated tartrate-Mg–Al layered double hydroxides," *Environmental Nanotechnology, Monitoring & Management*, vol. 1-2, pp. 2–7, 2014.

[45] T. P. Vogl, J. K. Mangis, A. K. Rigler, W. T. Zink, and D. L. Alkon, "Accelerating the convergence of the back-propagation method," *Biological Cybernetics*, vol. 59, no. 4-5, pp. 257–263, 1988.

[46] M. T. Hagan and M. B. Menhaj, "Training feedforward networks with the Marquardt algorithm," *IEEE Transactions on Neural Networks*, vol. 5, no. 6, pp. 989–993, 1994.

[47] M. T. Hagan, H. B. Demuth, and M. H. Beale, *Neural Network Design*, PWS Publishing, Boston, MA, 1996.

[48] P. E. Gill, W. Murray, and M. H. Wright, "Practical optimization," pp. 1–401, 1981.

[49] D. J. C. MacKay, "Bayesian interpolation," *Neural Computation*, vol. 4, no. 3, pp. 415–447, 1992.